Catal Lett (2008) 122:252–258
DOI 10.1007/s10562-008-9437-1

Propane Oxidative Dehydrogenation on V–Sb/ZrO_2 Catalysts

Silvana A. D'Ippolito · Miguel A. Bañares · José L. Garcia Fierro · Carlos L. Pieck

Received: 27 November 2007 / Accepted: 8 February 2008 / Published online: 26 February 2008

Abstract The catalytic properties of V–Sb/ZrO_2 and bulk Sb/V catalysts for the oxidative dehydrogenation of propane were studied. Samples were characterized by nitrogen adsorption, temperature-programmed reduction, temperature-programmed pyridine desorption and photoelectron spectroscopic techniques. Vanadia promotes the transition of tetragonal to monoclinic zirconia and the formation of ZrV_2O_7. Surface V and Sb oxide species do not appear to interact among them below monolayer coverage, but SbVO4 forms above monolayer. Simultaneously the excess of antimony forms α-Sb_2O_4. Activity and selectivity show no dependence on the acidity of the catalysts. However, there is a strong dependence of activity/selectivity on composition; surface vanadium species are active for propane oxidative dehydrogenation and the presence of Sb, affording rutile $VSbO_4$ phase makes the system selective to C_3H_6, this is believed to be related to the redox cycle involving dispersed V^{5+} species and lattice reduced vanadium site in the rutile $VSbO_4$ phase.

Keywords Oxidative dehydrogenation · Propane · V–Sb/ZrO_2

S. A. D'Ippolito · C. L. Pieck (✉)
Instituto de Investigaciones en Catálisis y Petroquímica, INCAPE (FIQ-UNL, CONICET), Santiago del Estero 2654, S3000AOJ Santa Fe, Argentina
e-mail: pieck@fiqus.unl.edu.ar

M. A. Bañares · J. L. G. Fierro
Instituto de Catálisis y Petroleoquímica, CSIC, Cantoblanco, Madrid 28049, Spain

1 Introduction

The oxidative dehydrogenation (ODH) of short chain alkanes (C_2–C_4) is studied as an alternative to non-oxidative dehydrogenation route to alkenes, which is carried out in presence of hydrogen at high temperatures (>600 °C). At these reaction conditions coking and cracking reactions also take place. Another hurdle in non-oxidative dehydrogenation is that reactions are endothermic, which makes it energy intensive. On the other hand, oxidative dehydrogenation is carried out in presence of oxygen, which reacts with the hydrogen eliminated from the alkane. The global reaction is now exothermic and, in addition, oxygen hinders the formation of coke. However alkenes are generally less stable than alkanes and therefore the oxidative dehydrogenation path has lower alkene selectivities due to the formation of combustion (CO and CO_2) products.

The ODH reaction of C_2–C_4 alkanes over supported transition metal oxides proceeds through a Mars-van-Krevelen mechanism that involves reduction of the catalyst by the alkane with participation of lattice oxygen followed by re-oxidation with oxygen [1]. Among the different catalysts used to promote the oxidative dehydrogenation of propane, supported vanadium oxide is among the most studied in the open bibliography [2–13]. Corma et al. [9] and Blasco and López et al. [10] proposed that the active sites for the oxidative dehydrogenation of alkanes are V^{5+} tetrahedral species. The presence of V^{4+} along V^{5+} is proposed as an important parameter for selectivity [11, 12] while the V^{4+}/V_{total} ratio does not appear to significantly affect conversion or selectivity [14]. It has also been reported that the V^{4+} ion in association with oxygen vacancies acts as an active species [13, 15]. A remarkable good performance in

butane ODH has been attributed to the good dispersion of V species, the presence of V^{4+} species and the pore structure [16]. It is well known that tetrahedral V is the active species but its environment remains controversial. The relevance of site isolation to make the system selective is apparently a key element [17, 18]. Alkene selectivity would be linked to isolated VO_4 tetrahedra [6, 7, 19–21] but others point to pyrovanadate structures [11, 22]. As the support has a great influence on both activity and selectivity [23, 24]. It has been proposed that active centres are of the V–O-support type [25]. Heracleous et al. [26] justify the higher activity of V catalysts supported on TiO_2 in comparison to V supported on Al_2O_3 by considering that the critical bond for the ODH reaction is the metal–O–support bond. The formation of polymeric entities with smaller chains (oligomers) is especially formed on the V/TiO_2 catalyst. The influence of the support on the reaction rate and selectivity has been attributed to acid-base properties of VO_x and the support [8, 10, 27, 28]. For a give support, e.g., alumina, the polymerization of surface vanadium oxide species affect their reducibility and generates new Brønsted acid sites [29]. In addition, bulk V_2O_5 appears responsible for non-selective oxidation of alkanes [29]. The selectivity trends appear closely related to the average oxidation state of the catalyst during reaction [6–10]. At the steady state, the surface of V_2O_5 is close to being fully oxidized and does not retain any strong acid sites. The surface vanadium oxide species remain essentially oxidized during propene ODH reaction on supported vanadium oxide catalysts [4]. To enhance the olefin selectivity, an optimum regeneration of the surface acidic properties and a rapid removal of the olefin from the reaction zone are essential. Owens and Kung [30] have emphasized the role of redox properties of the vanadium in determining the observed selectivity. In particular, the ease of oxygen removal from the lattice and the number of available lattice oxygen ions at the active site have been claimed to be the determining factor. The results of temperature-programmed reduction reported by Vèdrine et al. [31] show that silica-supported samples with dispersed vanadia undergo the reduction by hydrogen and ethane more easily than bulk V_2O_5 and silica-supported samples which contain crystalline V_2O_5.

Despite the numerous research works on propane ammoxidation using $SbVO_4$ as catalyst and the well-known fact than propene is one of the intermediate reaction products, few reports on the use of such catalysts for oxidative dehydrogenation of propane have been published to date [32, 33]. Therefore is of our interest to study the V–O and Sb–V–O systems supported on zirconia, since zirconia provides high reactivity to supported vanadia and V–Sb interaction modulates the redox properties of vanadium oxide species.

2 Experimental

2.1 Support

$Zr(OH)_4$ stabilized with 3.5% SiO_2 (MEL Chemical) was calcined at 650 °C in air to obtain ZrO_2.

2.2 $1V/ZrO_2$ Catalyst

It was prepared in a rotatory evaporator (Büchi 461). The support (ZrO_2), aqueous HNO_3 (pH = 2) and the required amount of NH_4VO_3 were processed at 80 °C under vacuum (0.7 atm) until dryness. The obtained powder was further dried in an oven at 120 °C overnight and finally calcined in air at 650 °C for 4 h. The catalyst was prepared with the objective of obtain a dispersed V monolayer. The monolayer content was calculated by considering a surface density of vanadium oxide of 9 V atoms per nm^2.

2.3 $1Sb/ZrO_2$ Catalysts

The Sb_2O_3 was kept in solution by means of chelation with tartaric acid and hence the preparation was the same that of the $1V/ZrO_2$ catalyst. Samples containing 1 monolayer of Sb were prepared.

2.4 $Sb–V/ZrO_2$ Catalysts

The ternary $Sb–V/ZrO_2$ catalysts, containing both V and Sb, were prepared by impregnating the support with aqueous solutions of the two oxides. The series were prepared with 0.5, 1.0 and 2.0 monolayers of Sb–V at a fixed atomic ratio of 3. The catalysts were named $0.5Sb\text{-}V/ZrO_2$, $1Sb\text{-}V/ZrO_2$, $2Sb\text{-}V/ZrO_2$, respectively.

A ZrV_2O_7 reference material was prepared by mixing aqueous NH_4VO_3 and the required amount of $Zr(OH)_4$ to have a V/Zr atomic ratio 2. Excess water was eliminated using a rotatory evaporator at the same conditions previously mentioned. Powder samples were dried at 120 °C overnight and then calcined 24 h at 700 °C.

2.5 Bulk Catalyst of Sb/V

Bulk $SbVO_4$ samples were prepared by mixing aqueous solutions of NH_4VO_3 and Sb_2O_3 of appropriate concentration in order to yield catalysts with Sb/V atomic ratios of 1 and 3. The drying and calcination steps were the same as

above. These catalysts were named Sb/V = 1 and Sb/V = 3, respectively.

2.6 X-ray Photoelectron

Spectra were recorded with a VG Escalab 200R electron spectrometer equipped with a hemispherical electron analyzer, using an MgKα ($h\nu$ = 1253.6 eV) X-ray source. The energy regions of V 2p–O 1s, Zr 3d and C 1s levels were scanned at a pass energy of 20 eV and signal-averaged for 90 scans. These conditions are appropriate for obtaining good signal-to-noise ratios. A PDP 11/04 computer (Digital) was used to record and analyze the spectra. Computing the integral of each peak was done after subtraction of an S-shaped background and fitting the experimental curve to a combination of Gaussian and Lorentzian lines estimated peak intensities. The C1s peak (contamination) at a binding energy (BE) of 284.9 eV was taken as an internal standard for BE measurements.

2.7 Temperature Programmed Reduction

A Micromeritics TPR/TPD 2000 equipment with a thermal-conductivity detector was used. The reducing medium was H_2 (5%) in Ar at 50 cm^3 min^{-1}. Temperature was linearly raised at 10 °C min^{-1}. Samples were previously heated at 150 °C under He for 1 h to eliminate residual moisture.

2.8 BET Area

It was determined by N_2 adsorption at −196 °C (BET method). Adsorption isotherms were obtained using a Micromeritics ASAP 2000 equipment. Samples were previously degassed at 140 °C during 2 h.

2.9 Temperature Programmed Pyridine Desorption

The quantity and strength of the surface acid sites of the catalysts were assessed by means of temperature programmed desorption of pyridine. 200 mg of the catalysts were immersed for 4 h in a closed vial containing pure pyridine (Merck, 99.9%). Then the catalyst was taken out from the vial and excess pyridine was removed by evaporation at room temperature under a fume hood. The sample was then charged to a quartz micro reactor with a constant nitrogen flow (40 cm^3/min). Weakly adsorbed pyridine was first desorbed in a first stage of stabilization by heating the sample at 110 °C for 2 h. The temperature of the oven was then raised to 600 °C at a heating rate of 10 °C min^{-1}. The reactor outlet was directly connected to a flame ionization detector to measure the desorption rate of pyridine.

2.10 Propane Oxidative Dehydrogenation

Runs were done using a quartz reactor with 50 mg catalysts samples. The reactor is a 7 mm i.d. quartz tube where void volume is minimized due to 6 mm O.D. quartz inserts. The reacting mixture was propane/oxygen/helium with a molar ratio of 1/2/4 at atmospheric pressure. The flow rate was kept at 30 cm^3 min^{-1} and the reaction temperature was varied in the range 340−640 °C. Products were analyzed using a gas chromatograph with a TCD.

3 Results and Discussion

3.1 Characterization of the Catalysts

Specific surface area and total acidity values as measured from pyridine programmed desorption tests are presented in Table 1. The ZrO_2 support has a specific surface of 86 m^2/g, and that the surface markedly diminishes with the deposition of a monolayer of V oxide. The addition of an Sb monolayer causes a lower decrease in surface area. Catalysts containing both V and Sb exhibit an intermediate behavior and it can be noted that the surface area diminishes as the V–Sb loading increases. Bulk catalysts have a low surface area that does not depend on the value of the Sb/V ratio. Reference ZrV_2O_7 has a very low surface area.

Regarding relative acidity values on a surface basis it can be concluded that the presence of V increases the acidity and that the presence of Sb decreases it. Mixed (Sb–V) supported catalysts shows again an intermediate behavior, its acidity being higher that the corresponding to the support alone. TPD traces are shifted to higher temperatures as catalyst loadings increase (results not shown). Finally, for the bulk catalysts, it can be pointed out that an increase in Sb/V ratio produces a decrease in acidity as a

Table 1 Specific surface area and specific (area and mass) pyridine desorption results taking the support as reference

Catalysts	Specific surface area (m^2/g)	Pyridine (a.u./g)	Pyridine (a.u./m^2)
Support	86	1.00	1.00
1V/ZrO_2	10	0.41	3.53
1Sb/ZrO_2	62	0.30	0.42
0.5V–Sb/ZrO_2	69	1.13	1.41
1V–Sb/ZrO_2	52	1.04	1.72
2V–Sb/ZrO_2	28	0.44	1.35
Sb/V = 1	6	0.19	2.72
Sb/V = 3	6	0.09	1.29
ZrV_2O_7	<1	0.00	0.00

consequence of the higher Sb amounts. These results are in accordance with those reported by Chiang and Lee [34], who found that the presence of Sb inhibits NH_3 adsorption on Sb–V catalysts. This could be due to an acidity decrease. Considering acidity values on a bulk basis, it can be observed that both the presence of Sb or V decreases the acidity which can be explained taking into account the strong decrease in the ZrO_2 surface area caused by Sb or V addition.

Previously we published some results of TPR experiment of V/ZrO_2 calcined at 650 °C and pure V_2O_5 [35]. It was found that vanadium oxide exhibits three reduction peaks at 654, 687 and 806 °C was attributed to the consecutive reduction steps of V from V_2O_5–V_2O_3. Similar results were reported by Bosch et al. [36] and Koranne et al. [37]. Regarding the supported catalysts TPR traces the lower V reduction temperatures (482, 572 and 606 °C) of V/ZrO_2 compared to pure V_2O_5 (653, 684 and 806 °C) were noticeable. From these results it was concluded that the support V had the presence of both disperse and crystalline V [37].

The reduction profiles for mixed Sb–V bulk and supported catalysts are shown in Fig. 1. The reduction pattern of Sb_2O_3 and $1Sb/ZrO_2$ shown that Sb_2O_3 reduces near 600 and 690 °C while $1Sb/ZrO_2$ catalyst exhibits a unique reduction peak occurring at a temperature (535 °C) lower than that of crystalline Sb_2O_3 (Fig. 1). The reduction of $0.5Sb–V/ZrO_2$ catalysts occurs in a wide temperature range (300–550 °C). The $1Sb–V/ZrO_2$ catalyst has a unique reduction peak at 520 °C and catalysts the $2Sb–V/ZrO_2$ catalysts have two peaks at 538 and 566 °C. These reduction peaks are located at lower temperatures than those of the pure metal oxides. They are thus attributed the reduction of surface species and not to the reduction of bulk vanadium and antimony oxide crystals. Bulk catalysts reduce at higher temperatures than the supported ones. The reduction peaks shift to higher temperatures with the Sb/V ratio.

The XRD and Raman spectra of the catalysts were published elsewhere [38]. The main peak of each catalyst is reported in Table 2. Based on XRD patterns, the support calcined at 650 °C has a 100% tetragonal phase, because of the presence of a 30.5° peak and the absence of the 28.2° and 31.5° ones, related to the monoclinic phase [39]. We also reported that the incorporation of V causes a transformation of zirconia into a fully monoclinic phase and the occurrence of diffraction peaks at 16, 20, 22.5 and 24.8° due to ZrV_2O_7 formation. On the contrary, the presence of Sb does not induce any transformation in the crystalline structure of zirconia. However a new peak appears at 28.2° that corresponds to α-Sb_2O_3 (valentinite). The ZrO_2 crystal phase in V and Sb supported catalysts was tetragonal at any V or Sb loadings except for lower Sb–V loadings where

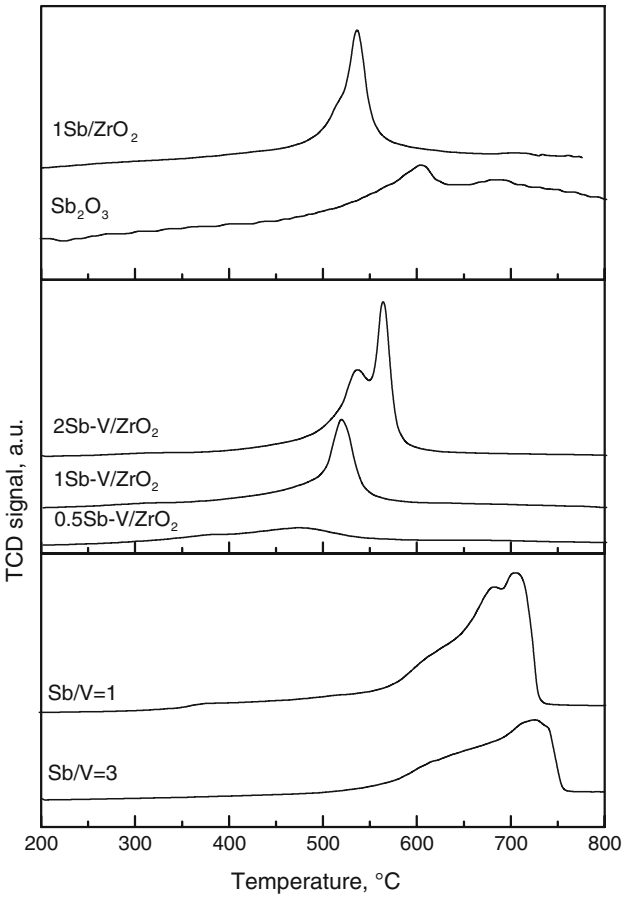

Fig. 1 TPR traces of Sb_2O_3 pure oxide, $1Sb/ZrO_2$, $V–Sb/ZrO_2$ (supported) and Sb/V (bulk) catalysts

little amounts of monoclinic phase were observed. For this catalyst, no peaks corresponding to ZrV_2O_7 were observed. It was also found that the bulk catalyst with an Sb/V ratio of 1 had peaks at 27.5, 35.3, 39.3, 40.5, 53.8, 56.1, 65.1 and 68.7° that correspond to the $VSbO_4$, rutile-type phase. Two tiny peaks at 25.8° and 29° were also detected and they were attributed to the Sb_2O_4 cervantite phase. Regarding the sample with $Sb/V = 3$ it is evident that the $VSbO_4$ phase is accompanied by Sb_2O_4 and α-Sb_2O_4 cervantite because the peaks at 25.8 and 29° were more intense. The XRD data of the bulk catalysts were in agreement with those reported by Nilsson et al. [40]. They reported that bulk Sb–V with high Sb/V ratio exhibited a $SbVO_4$ rutile-type structure and that the excess of Sb produced superficial α-Sb_2O_4 while catalysts with lower Sb/V contained crystalline V_2O_5.

The samples were also characterized by Raman spectroscopy [38]. It was reported that the support was 100% tetragonal, as indicated by the Raman bands at 263, 325, 472, 608 and 640 cm^{-1}, in agreement with the XRD patterns. The addition of vanadia produced a transition to the monoclinic phase (new modes near 175, 190, and 477 cm^{-1}). It was also

Table 2 RD and Raman peaks

Catalysts	XRD		Raman	
	Main peaks,°	Observations	Main peaks, cm^{-1}	Observations
Support	30.5	T	263, 325, 472, 608, 640	T
$1V/ZrO_2$	28.2, 31.5	M	175, 190, 477	M
	16, 20, 22.5, 24.8	ZrV_2O_7	1030	V disperse
			990, 780	ZrV_2O_7
			143, 283, 302, 405, 526, 698, 994	V_2O_5 crystal
$1Sb/ZrO_2$	30.5	T	175, 190, 263, 325, 477, 608, 640	T and M
	28.2	α-Sb_2O_3 (valentite)		
0.5V- Sb/ZrO_2	30.5	T and M	452, 750, 950	$SbVO_4$
	28.2, 31.5		190, 400	α-Sb_2O_4
1V- Sb/ZrO_2	30.5	T	452, 750, 950	$SbVO_4$
			190, 400	α-Sb_2O_4
			1030	V disperse
2V- Sb/ZrO_2	30.5	T	452, 750, 950	$SbVO_4$
			190, 400	α-Sb_2O_4
			1030	V disperse
Sb/V = 1	27.5, 35.3, 39.3, 40.5, 53.8, 56.1, 65.1, 68.7	$SbVO_4$	143, 283, 523, 694, 994	V_2O_5
	25.8, 29.0	Sb_2O_4 cervantite		
Sb/V = 3	27.5, 35.3, 39.3, 40.5, 53.8, 56.1, 65.1, 68.7	$SbVO_4$	190, 397	α-Sb_2O_4
	25.8, 29.0	Sb_2O_4 cervantite and α-Sb_2O_4 cervantite	750, 950	$SbVO_4$

ZrO_2 phases: T: tetragonal, M: monoclinic

reported that the band at 1030 cm^{-1} is sensitive to hydration, confirming that it belongs to dispersed vanadium oxide species since crystals are not sensitive to hydration treatments [41]. The Raman measurements reveal that vanadia is dispersed on the zirconia support (1030 cm^{-1}) and that ZrV_2O_7 is formed (990, 780 cm^{-1}). It was also possible to detect the formation of V_2O_5 crystals (Raman bands at 143, 283, 302, 405, 526, 698 and 994 cm^{-1}). No Sb oxide bands are evident in the spectra of $1Sb/ZrO_2$ catalysts and bands due to both tetragonal and monoclinic zirconia were detected. The Sb–V/ZrO_2 catalysts maintain the tetragonal structure at high loadings although the monoclinic phase is observed at low SbV contents. The broad band at 750–950 cm^{-1} and the band at 452 cm^{-1} were ascribed to the appearance of the $SbVO_4$ phase in agreement with Nilsson et al. [42, 43]. Thus, at low coverage, the V–Sb/ZrO_2 system has dispersed antimony oxide, dispersed vanadium oxide, and bulk $SbVO_4$. As the Sb–V coverage increases, the formation of $SbVO_4$ is revealed by new Raman bands at about 452 and 760 cm^{-1} and by the decrease of the band due to dispersed vanadium oxide species (1,030 cm^{-1}). The excess of Sb forms α-Sb_2O_4 with broad Raman bands at about 190 and 400 cm^{-1}. The spectra of 1Sb–V/ZrO_2 and 0.5Sb–V/ZrO_2 exhibit Raman bands due to Sb_2O_4 (190 and 400 cm^{-1}), dispersed vanadium oxide (1,030 cm^{-1}), $SbVO_4$ (750–950 and 452 cm^{-1}) and the monoclinic phase of ZrO_2.

Finally, bulk Sb/V = 3 oxide exhibits Raman bands at 190 and 397 cm^{-1}, characteristic of α-Sb_2O_4, and a broad peak at 750–950 cm^{-1}, presumably due to the presence of the rutile-type phase of $SbVO_4$. On the contrary $SbVO_4$ (i.e. Sb/V = 1) showed peaks at 143, 283, 523, 694 and 994 cm^{-1}, related to V_2O_5.

Surface atomic ratios as obtained from XPS spectra are presented in Table 3. The V/Zr and Sb/Zr XPS intensity ratios of the supported catalysts had higher values than those corresponding to the bulk one, as expected for supported oxides. The supported catalysts exhibited also Sb/V atomic ratios which were lower than the theoretical ones, indicating a surface enrichment in V. This phenomenon can be explained taking into account the stronger interaction of vanadia on a zirconia support. The same trend is observed for supported Sb/V catalysts. Conversely, the bulk catalysts exhibited Sb/V XPS ratios above the bulk stoichiometry.

3.2 Oxidative Dehydrogenation of Propane

Values of conversion obtained in the oxidative dehydrogenation tests are shown in Fig. 2. It must be noted that the oxidative dehydrogenation activity of the ZrV_2O_7 reference

Table 3 V/Zr, Sb/Zr and Sb/V atomic ratios as obtained by XPS analysis

Catalysts	(V/Zr) bulk	(V/Zr) XPS	(Sb/Zr) bulk	(Sb/Zr) XPS	(Sb/V) XPS
$1V/ZrO_2$	0.135	0.253			
$1Sb/ZrO_2$			0.135	0.479	
$0.5Sb\text{-}V/ZrO_2$	0.017	0.051	0.051	0.104	2.04
$1Sb–V/ZrO_2$	0.034	0.098	0.102	0.200	2.04
$2Sb–V/ZrO_2$	0.068	0.192	0.204	0.559	2.91
Sb/V = 1					1.19
Sb/V = 3					3.34

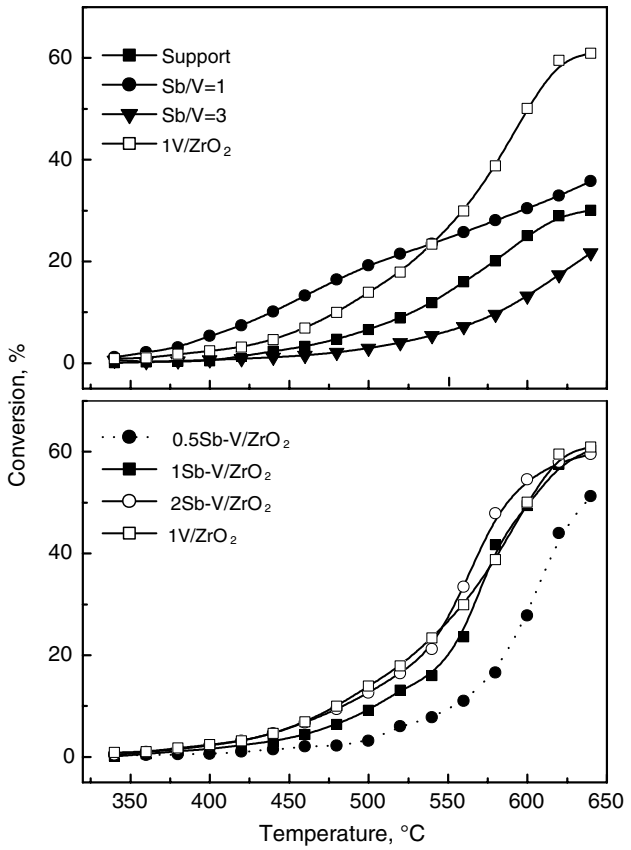

Fig. 2 Propane oxidative dehydrogenation. Conversion as a function of reaction temperature

sample is very low (0.5% at 600 °C) and the same holds for the $1Sb/ZrO_2$ catalyst (5% conversion and 5% propene selectivity at 600 °C). Both had a lower activity than the unpromoted support.

The lower activity of the ZrV_2O_7 reference sample has been previously reported [14]. Figure 2 shows that the $1V/ZrO_2$ catalyst is more active than its support. This reflects the higher intrinsic activity of surface vanadium oxide species. The inhibiting effect of Sb on catalytic activity is also observed in bulk catalysts; the bulk catalyst with an Sb/V = 3 atomic ratio has lower activity than the one with Sb/V = 1. In both series, the activity trends do not follow the acidity trends, determined by pyridine adsorption. Note that total vanadium loading is the same for $1V/ZrO_2$ and $2V–Sb/ZrO_2$. Thus, it is apparent that total activity depends on vanadia loading, and Sb–V interaction does not appear to be critical for propane conversion. Vanadium oxide species undergo a redox cycle between lattice reduced sites and dispersed V^{5+} species that is operative for propane ammoxidation [44], and which appears operative for propane oxidative dehydrogenation, according to the present results. However, an excess of antimony would "sequestrate" vanadium species, limiting its availability for ODH reaction.

Propene selectivity versus conversion curves are shown in Fig. 3. Plots for $1Sb/ZrO_2$ and ZrV_2O_7 are not shown since these materials have low activities and selectivities. Typical consecutive reaction curves were obtained, i.e. intermediate product selectivity decreases as conversion increases. The bulk catalyst with Sb/V = 3 has a higher propene selectivity than the one with Sb/V = 1 and ZrO_2. For supported catalysts and for lower (<10%) conversions,

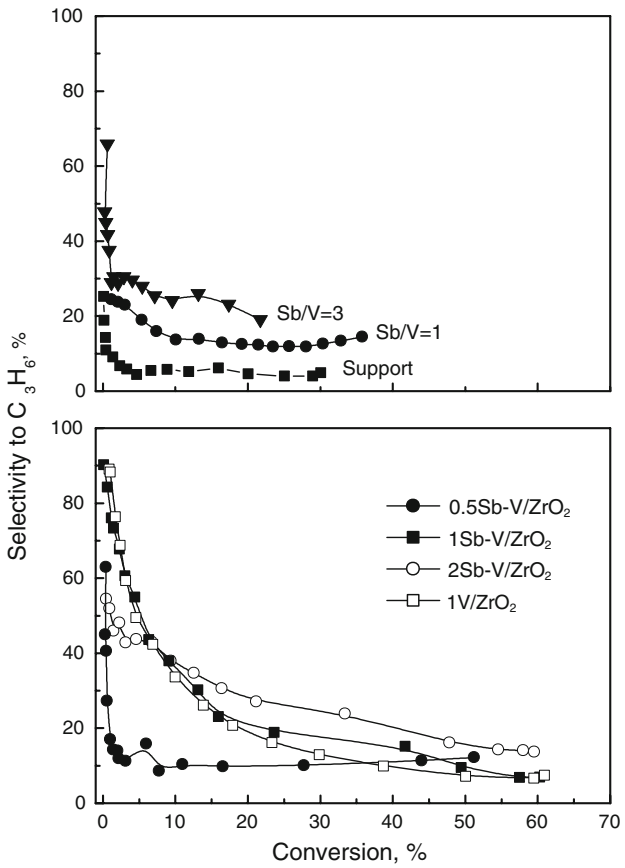

Fig. 3 Propane oxidative dehydrogenation. Propene selectivity versus conversion curves

best (and comparable) selectivities were found for $1V/ZrO_2$ and $1Sb–V/ZrO_2$. For higher conversion values, the $2Sb–V/ZrO_2$ catalyst affords the highest propene selectivity. The selectivity trend shows no correspondence with acidity trends, measured by pyridine adsorption. Characterization results show that as the Sb/V ratio increased, both segregated Sb oxide species and $SbVO_4$ become increasingly dominant. Note that total vanadium loading is the same for $1V/ZrO_2$ and $2V–Sb/ZrO_2$; however, propylene selectivity is significantly higher for $2V–Sb/ZrO_2$, which indicates that the V–Sb interaction renders the system more selective to propylene. This would be related to a different behaviour of vanadium species, probably participating in a redox cycle between dispersed V^{5+} and lattice reduced vanadium sites in rutile $VSbO_4$. Such an interaction, renders vanadium species isolated within the rutile latttice, thus underlining that vanadium site isolation is important for selective oxidation of propane to propylene; while it would not affect total activity.

4 Conclusions

The simultaneous presence of Sb and V on zirconia at low coverage leads to a preferential interaction of individual V and Sb oxides on the zirconia surface rather than forming a binary Sb–V oxide. Pyridine adsorption shows that this interaction affects acidity; however, acidity trends do not reflect on total activity or selectivity for propane oxidative dehydrogenation to propylene. Total vanadium loading appears critical for total propane conversion values. The vanadium-antimony oxide species interaction leads to rutile $SbVO_4$ phases, where vanadium sites isolate within this lattice, and participate in a redox cycle between lattice-reduced sites and dispersed V^{5+} species. The presence of Sb has no effect on total conversion; except at higher Sb/V ratios, when in addition to $SbVO_4$, excess of antimony forms α-Sb_2O_4. The presence of Sb, does have a promoting effect on selectivity to propylene. Thus, site isolation provided by the rutile $VSbO_4$ phase may account for an increase in selectivity. Still, total activity would not be affected by the presence of antimony.

References

1. Mars P, Van Krevelen DW (1954) Chem Eng Sci 3:41
2. Chen K, Khodakov A, Yang J, Bell J, Iglesia E (1999) J Catal 186:325
3. Gao X, Jehng J, Wachs J (2002) J Catal 2009:43
4. Garcia Cortez G, Bañares G (2002) J Catal 209:197
5. Chen K, Bell AT, Iglesia E (2002) J Catal 209:35
6. Khodakov A, Olthof B, Bell AT, Iglesia E (1999) J Catal 181:205
7. Khodakov A, Yang J, Su S, Iglesia E, Bell AT (1998) J Catal 177:343
8. Mamedov EA, Cortés corberán EA (1995) Appl Catal A 127:1
9. Corma A, López Nieto JM, Paredes N, Peréz M, Shen M, Cao H, Suib H (1992) Stud Surf Sci Catal 72:213
10. Blasco T, López Nieto JM (1997) Appl Catal A 157:117
11. Siew Hew Sam D, Soenen V, Volta JC (1990) J Catal 123:417
12. Chaar MA, Patel D, Kung MC, Kung HH (1987) J Catal 105:483
13. Pieck CL, Bañares MA, Fierro JLG (2004) J Catal 224:1
14. Guerrero Ruiz A, Rodriguez Ramos I, Fierro JLG, Soenen V, Herman JM, Volta JC (1992) Stud Surf Sci Catal 72:203
15. Zhanga W, Aub C, Wan H (1999) Appl Catal A 181:63
16. Liu W, Lai SY, Dai H, Wang S, Sun H, Au CT (2007) Catal Lett 113:147
17. Schubert UA, Anderle F, Spengler J, Zühlke J, Eberle HJ, Grasselli RK, Knözinger H (2001) Top Catal 15:195
18. Spengler J, Anderle F, Bosch RK, Grasselli E, Pillep E, Behrens P, Lapina OB, Shubin AA, Eberle HJ, Knözinger H (2001) J Phys Chem B 105:10772
19. Corma A, López Nieto A, Paredes N (1993) J Catal 1444:425
20. Michalakos PM, Kung MC, Jahan I, Kung HH (1993) J Catal 140:226
21. Argyle MD, Chen K, Bell AT, Iglesia E (2002) J Catal 208:139
22. Lindblad T, Rebenstorf B, Yan ZG, Andersson SLT (1994) Appl Catal A 112:187
23. Routray K, Reddy KRSK, Deo G (2004) Appl Catal A 265:103
24. Kondratenko EV, Cherian M, Baerns M (2006) Catal Today 112:60
25. Smits RHH, Seshan K, Leemresize H, Ross JRH (1993) Catal Today 16:513
26. Heracleous E, Machli M, Lemonidou AA, Vasalos IA (2005) J Mol Catal A Chem 232:29
27. Khodakov A, Yang J, Su S, Iglesia E, Bell AT (1998) J Catal 177:343
28. Chen KD, Khodakov A, Yang J, Bell AT, Iglesia E (1999) J Catal 186:325
29. Martínez-Huerta MV, Gao X, Tian H, Wachs IE, Fierro JLG, Bañares MA (2006) Catal Today 118:279
30. Owens L, Kung HH (1993) J Catal 144:202
31. Le Bars J, Auroux A, Védrine JC, Baerns M (1992) Stud Surf Sci Catal 72:181
32. Juárez López R, Godjayeva NS, Córtes Corberán V, Fierro JLG, Manedod EA (1995) Appl Catal A 124:281
33. Stelzer JB, Caro J, Fait M (2005) Catal Comm 6:1
34. Chiang H, Lee M (1997) Appl Catal A 154:55
35. Pieck CL, Del Val S, López Granados M, Bañares MA, Fierro JLG (2002) Langmuir 18:2642
36. Bosch H, Kip BJ, van Ommen JG, Gellings PJ (1984) J Chem Soc Faraday Trans 1(80):2479
37. Koranne MM, Goodwin JG Jr, Marcelin G (1994) J Catal 148:369
38. Pieck CL, Bañares MA, Vicente MA, Fierro JLG (2001) Chem Mat 13:1174
39. Selected power difraction data for metals and alloys. Data Book, 1st edn, vol II, cards No. 13-307 and No 24-1164. International Center for Difraction Data (JCPDS), Swarthmore, USA
40. Nilsson R, Lindblad T, Andersson A (1994) J Catal 148:501
41. Wachs IE (1996) Catal Today 27:437
42. Nilsson R, Lindblad T, Andersson A, Song C, Hansen S (1994) Stud Surf Sci Catal 82:293
43. Nilsson R, Lindblad T, Andersson A (1994) J Catal 148:501
44. Guerrero-Pérez MO, Bañares MA (2007) J Phys Chem C 111:1315